The applied field $\mathbf{E}_0$ generates oscillation of an electric dipole in a fixed direction. The oscillating dipole, in turn, produces a plane-polarized electromagnetic wave, the scattered wave. To evaluate the scattered electric field in regions that are far away from the dipole, we let $r$ denote the distance between the dipole and the observation point, $\gamma$ the angle between the scattered dipole moment $\mathbf{p}$ and the direction of observation, and $c$ the velocity of light. According to the classical electromagnetic solution given by Hertz (1889), the scattered electric field is proportional to the acceleration of the scattered dipole moment and $\sin \gamma$, but is inversely proportional to the distance $r$. Thus, we have

$$\mathbf{E} = \frac{1}{c^2} \frac{1}{r} \frac{\partial^2 \mathbf{p}}{\partial t^2} \sin \gamma. \tag{3.3.2}$$

In an oscillating periodic field, the scattered dipole moment may be written in terms of the induced dipole moment as

$$\mathbf{p} = \mathbf{p}_0 e^{-ik(r-ct)}. \tag{3.3.3}$$

Note that $k$ is the wavenumber, and $kc = \omega$ is the circular frequency. By combining Eqs. (3.3.1) and (3.3.3), Eq. (3.3.2) yields

$$\mathbf{E} = -\mathbf{E}_0 \frac{e^{-ik(r-ct)}}{r} k^2 \alpha \sin \gamma. \tag{3.3.4}$$

Now we consider the scattering of sunlight by air molecules. Let the plane defined by the directions of incident and scattered waves be the reference plane (plane of scattering). Since any electric vector may be arbitrarily decomposed into orthogonal components, we may choose the two components perpendicular ($E_r$) and parallel ($E_l$) to the plane of scattering. The sunlight is characterized by the same electric field in the $r$ and $l$ directions and by a random phase relation between these two components, and is referred to as *natural* or *unpolarized* light (see Section 6.6 for a more advanced discussion of the representation of polarized light). In this case, we may consider separately the scattering of the two electric field components $E_{0r}$ and $E_{0l}$ by molecules assumed to be homogeneous, isotropic, spherical particles. Based on Eq. (3.3.4), we have

$$E_r = -E_{0r} \frac{e^{-ik(r-ct)}}{r} k^2 \alpha \sin \gamma_1, \tag{3.3.5a}$$

$$E_l = -E_{0l} \frac{e^{-ik(r-ct)}}{r} k^2 \alpha \sin \gamma_2. \tag{3.3.5b}$$

Referring to Fig. 3.10, we see that $\gamma_1 = \pi/2$ and $\gamma_2 = \pi/2 - \Theta$, where $\Theta$ is defined as the scattering angle, which is the angle between the incident and scattered waves. Note that $\gamma_1$ is always equal to $90°$ because the scattered dipole moment (or the scattered electric field) in the $r$ direction is normal to the scattering plane defined previously.

In matrix form, we may write

$$\begin{bmatrix} E_r \\ E_l \end{bmatrix} = -\frac{e^{-ik(r-ct)}}{r} k^2 \alpha \begin{bmatrix} 1 & 0 \\ 0 & \cos \Theta \end{bmatrix} \begin{bmatrix} E_{0r} \\ E_{0l} \end{bmatrix}. \tag{3.3.6}$$
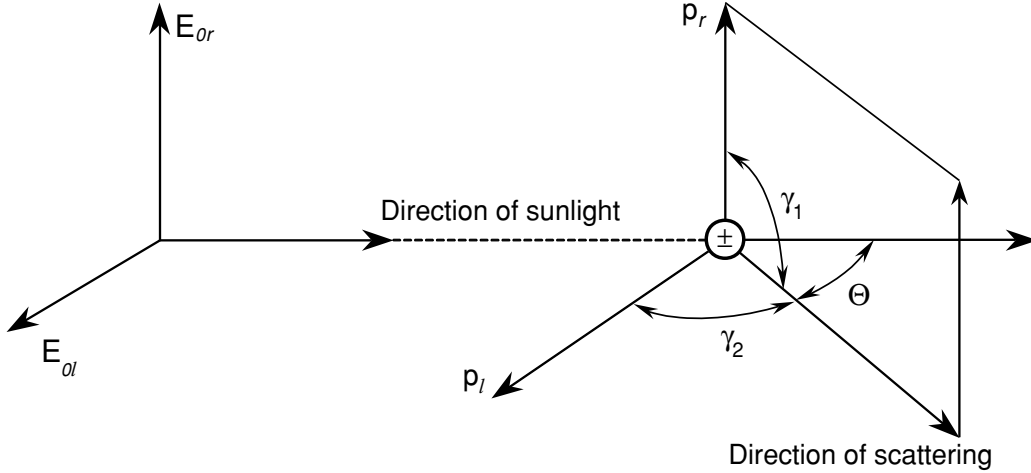
**Figure 3.10** Scattering by a dipole. The incident electric field, a vector, can be arbitrarily decomposed into a parallel (*l*) and a perpendicular (*r*) component, where each undergoes the scattering by the dipole. We may select the component that is always perpendicular to the scattering plane that is defined by the incident and scattering beams (i.e., $\gamma_1 = 90°$). All the notations are defined in the text.

A complete description of the intensity of a light beam and its polarized state will be given in Section 6.6 in which the Stokes parameters are introduced. For the sake of the continuity of the present discussion, however, we may define the intensity components (per solid angle) of the incident and scattered radiation in the forms $I_0 = C|E_0|^2$ and $I = C|E|^2$, where $C$ is a certain proportionality factor such that $C/r^2$ implies a solid angle. It follows that Eqs. (3.3.5) and (3.3.6) can be expressed in the form of intensities as

$$I_r = I_{0r}k^4\alpha^2/r^2, \tag{3.3.7a}$$

$$I_l = I_{0l}k^4\alpha^2 \cos^2\Theta/r^2, \tag{3.3.7b}$$

where $I_r$ and $I_l$ are polarized intensity components perpendicular and parallel to the plane containing the incident and scattered waves, i.e., the plane of scattering. The total scattered intensity of the unpolarized sunlight incident on a molecule in the direction of $\Theta$ is then

$$I = I_r + I_l = (I_{0r} + I_{0l}\cos^2\Theta)k^4\alpha^2/r^2. \tag{3.3.8}$$

But for unpolarized sunlight, $I_{0r} = I_{0l} = I_0/2$, and by noting that $k = 2\pi/\lambda$, we obtain

$$I = \frac{I_0}{r^2}\alpha^2\left(\frac{2\pi}{\lambda}\right)^4 \frac{1+\cos^2\Theta}{2}. \tag{3.3.9}$$

This is the original formula derived by Rayleigh, and we call the scattering of sunlight by molecules *Rayleigh scattering*. By this formula, the intensity of unpolarized sunlight scattered by a molecule is proportional to the incident intensity $I_0$ and is inversely proportional to the square of the distance between the molecule and the

point of observation. In addition to these two factors, the scattered intensity also depends on the polarizability, the wavelength of the incident wave, and the scattering angle. The dependence of these three parameters on the scattering of sunlight by molecules introduces a number of significant physical features.

### 3.3.1.2  PHASE FUNCTION, SCATTERING CROSS SECTION, AND POLARIZABILITY

On the basis of Eqs. (3.3.7) and (3.3.9), the intensity scattered by a molecule depends on the polarization characteristics of the incident light. For vertically ($r$) polarized incident light, the scattered intensity is independent of the direction of the scattering plane. In this case then, the scattering is isotropic. On the other hand, for horizontally ($l$) polarized incident light, the scattered intensity is a function of $\cos^2 \Theta$. When the incident light is unpolarized, such as sunlight, the scattered intensity depends on $(1 + \cos^2 \Theta)$. The angular scattering patterns in space for the three types of incident polarization are illustrated in Fig. 3.11. We see that the scattering of unpolarized sunlight by molecules (Rayleigh scattering) has maxima in the forward ($0°$) and backward ($180°$) directions, whereas it shows minima in the side directions ($90°$ and $270°$). Light scattered by particles or molecules is not confined only to the plane of incidence, but is visible in all azimuthal directions. Because of the spherical symmetry assumed for molecules, scattering patterns are symmetrical in three-dimensional space, as demonstrated in Fig. 3.11.

To describe the angular distribution of scattered energy in conjunction with multiple scattering and radiative transfer analyses and applications for planetary atmospheres, we find it necessary to define a nondimensional parameter called the *phase function, $P(\cos \Theta)$,* such that

$$\int_0^{2\pi} \int_0^{\pi} \frac{P(\cos \Theta)}{4\pi} \sin \Theta \, d\Theta \, d\phi = 1. \tag{3.3.10}$$

By this definition, the phase function is said to be normalized to unity. Upon performing simple integrations, the phase function of Rayleigh scattering for incident unpolarized sunlight is given by

$$P(\cos \Theta) = \frac{3}{4}(1 + \cos^2 \Theta). \tag{3.3.11}$$

Employing the definition of the phase function, Eq. (3.3.9) may be rewritten in the form

$$I(\Theta) = \frac{I_0}{r^2} \alpha^2 \frac{128\pi^5}{3\lambda^4} \frac{P(\Theta)}{4\pi}. \tag{3.3.12}$$

It follows that the angular distribution of the scattered intensity is directly proportional to the phase function.

The scattered flux $f$ (or power, in units of energy per time) can be evaluated by integrating the scattered flux density ($I \Delta\Omega$) over the appropriate area a distance $r$
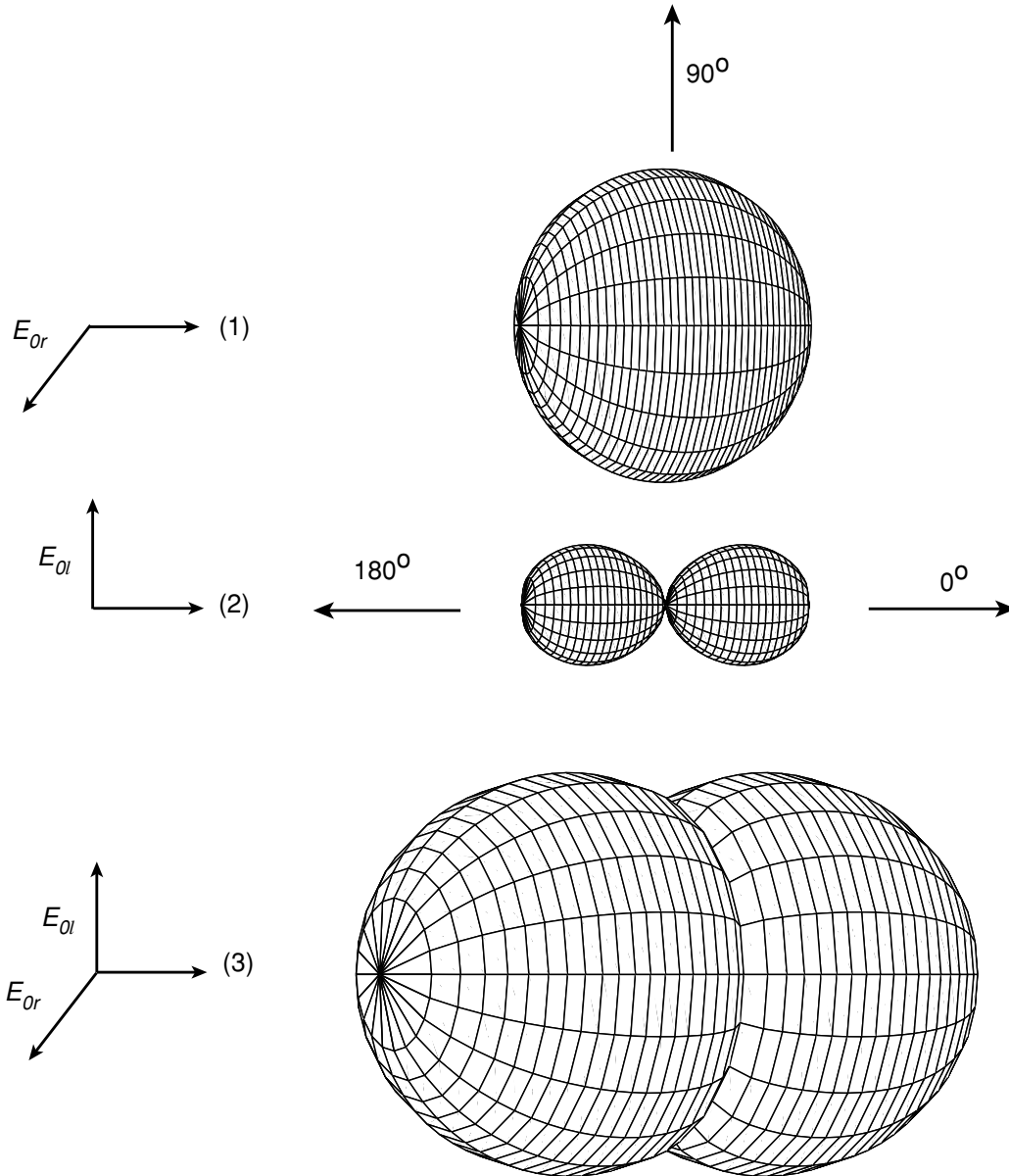
**Figure 3.11**   Polar diagram of the scattered intensity for Rayleigh molecules: (1) polarized incident light with the electric vector perpendicular to the scattering plane, (2) polarized incident light with the electric vector on the scattering plane, and (3) unpolarized incident light.

away from the scatterer. Thus,

$$f = \int_{\Omega} (I \, \Delta\Omega) r^2 \, d\Omega, \tag{3.3.13a}$$

where $r^2 d\Omega$ represents the area according to the definition of the solid angle. Inserting the expressions for scattered intensity and the differential solid angle defined in Eqs. (3.3.12) and (1.1.5), respectively, into Eq. (3.3.13a) and carrying out integrations over the solid angle of a sphere, we obtain the equivalent isotropically scattered flux

in the form

$$f = F_0 \alpha^2 128 \pi^5/(3\lambda^4), \tag{3.3.13b}$$

where the incident flux density $F_0$ is equal to $I_0 \Delta\Omega$. Moreover, we may define the scattering cross section per one molecule as

$$\sigma_s = f/F_0 = \alpha^2 128 \pi^5/(3\lambda^4). \tag{3.3.14}$$

The scattering cross section (in units of area) represents the amount of incident energy that is removed from the original direction because of a single scattering event such that the energy is redistributed isotropically on the area of a sphere whose center is the scatterer and whose radius is $r$. In terms of the scattering cross section, the scattered intensity can be expressed by

$$I(\Theta) = I_0 \frac{\sigma_s}{r^2} \frac{P(\Theta)}{4\pi}. \tag{3.3.15}$$

This is the general expression for scattered intensity, which is valid not only for molecules but also for particles whose size is larger than the incident wavelength, as will be discussed in Section 5.2.

The *polarizability* $\alpha$, which was used in the preceding equations, can be derived from the principle of the dispersion of electromagnetic waves and is given by

$$\alpha = \frac{3}{4\pi N_s} \left( \frac{m^2 - 1}{m^2 + 2} \right), \tag{3.3.16}$$

where $N_s$ is the total number of molecules per unit volume and $m$ is the nondimensional refractive index of molecules. This equation is called the *Lorentz–Lorenz formula,* and its derivation is given in Appendix D. The refractive index is an optical parameter associated with the velocity change of electromagnetic waves in a medium with respect to a vacuum. Its definition and physical meanings are also given in Appendix D. Normally, the refractive indices of atmospheric particles and molecules are composed of a real part $m_r$ and an imaginary part $m_i$ corresponding, respectively, to the scattering and absorption properties of particles and molecules. In the solar visible spectrum, the imaginary parts of the refractive indices of air molecules are so insignificantly small that absorption of solar radiation by air molecules may be neglected in the scattering discussion. The real parts of the refractive indices of air molecules in the solar spectrum are very close to 1, but they depend on the wavelength (or frequency) of the incident radiation as illustrated in Appendix D. Because of this dependence, white light may be *dispersed* into component colors by molecules that function like prisms. The real part of the refractive index derived in Appendix D [(Eq. D.17)] may be approximately fitted by

$$(m_r - 1) \times 10^8 = 6432.8 + \frac{2,949,810}{146 - \lambda^{-2}} + \frac{25,540}{41 - \lambda^{-2}}, \tag{3.3.17}$$

where $\lambda$ is in units of micrometers. Since $m_r$ is close to 1, for all practical purposes, Eq. (3.3.16) may be approximated by

$$\alpha \approx \frac{1}{4\pi N_s}\left(m_r^2 - 1\right).$$

(3.3.18)

Thus, the scattering cross section defined in Eq. (3.3.14) becomes

$$\sigma_s = \frac{8\pi^3\left(m_r^2 - 1\right)^2}{3\lambda^4 N_s^2} f(\delta).$$

(3.3.19)

A correction factor $f(\delta)$ is added in Eq. (3.3.19) to take into consideration the anisotropic property of molecules, where $f(\delta) = (6 + 3\delta)/(6 - 7\delta)$ with the anisotropic factor $\delta$ of 0.035. Anisotropy implies that the refractive index of molecules varies along the $x$, $y$, and $z$ directions, and thus is a vector, not a scalar. Hence, the polarizability $\alpha$ is a tensor, as noted previously.

The optical depth of the entire molecular atmosphere at a given wavelength may be calculated from the scattering cross section in the form

$$\tau(\lambda) = \sigma_s(\lambda) \int_0^{z_\infty} N(z)\,dz,$$

(3.3.20)

where $N(z)$ denotes the number density of molecules as a function of height, and $z_\infty$ is the top of the atmosphere. The optical depth represents the attenuation power of molecules with respect to a specific wavelength of the incident light. Exercises 3.7–3.11 require the calculation of a number of parameters based on Rayleigh scattering results.

### 3.3.1.3 BLUE SKY AND SKY POLARIZATION

Returning to Eq. (3.3.12), we see that the scattered intensity depends on the wavelength of incident light and the index of refraction of air molecules contained in the polarizability term. According to the analyses given in Appendix D and Eq. (3.3.17), the index of refraction also depends slightly on the wavelength. However, the dependence of the refractive index on the wavelength is relatively insignificant in calculating the scattered intensity as compared to the explicit wavelength term. Thus, the intensity scattered by air molecules in a specific direction may be symbolically expressed in the form

$$I_\lambda \sim 1/\lambda^4.$$

(3.3.21)

The inverse dependence of the scattered intensity on the wavelength to the fourth power is a direct consequence of the theory of Rayleigh scattering and is the foundation for the explanation of blue sky.

In reference to the observed solar energy spectrum displayed in Fig. 3.9, a large portion of solar energy is contained between the blue and red regions of the visible spectrum. Blue light ($\lambda \approx 0.425\ \mu$m) has a shorter wavelength than red light ($\lambda \approx 0.650\ \mu$m). Consequently, according to Eq. (3.3.21) blue light scatters about 5.5 times

more intensity than red light. It is apparent that the $\lambda^{-4}$ law causes more blue light to be scattered than red, green, and yellow, and so the sky, when viewed away from the sun's disk, appears blue. Moreover, since molecular density decreases drastically with height, it is anticipated that the sky should gradually darken to become completely black in outer space in directions away from the sun. And the sun itself should appear whiter and brighter with increasing height. As the sun approaches the horizon (at sunset or sunrise), sunlight travels through more air molecules, and therefore more and more blue light and light with shorter wavelengths are scattered out of the beam of light, and the luminous sun shows a deeper red color than at its zenith. However, since violet light ($\sim$0.405 $\mu$m) has a shorter wavelength than blue, a reasonable question is, why doesn't the sky appear violet? This is because the energy contained in the violet spectrum is much less than that contained in the blue spectrum, and also because the human eye has a much lower response to the violet color.

Another important phenomenon explained by the Rayleigh scattering theory is sky polarization. For many atmospheric remote sensing applications utilizing polarization, a parameter called the *degree of linear polarization* has been used (Subsection 7.3.5.2). In the case of Rayleigh scattering it is given by

$$LP(\Theta) = -\frac{I_l - I_r}{I_l + I_r} = -\frac{\cos^2 \Theta - 1}{\cos^2 \Theta + 1} = \frac{\sin^2 \Theta}{\cos^2 \Theta + 1}. \qquad (3.3.22)$$

In the forward and backward directions the scattered light remains completely unpolarized, whereas at the 90° scattering angle, the scattered light becomes completely polarized. In other directions, the scattered light is partially polarized with the percentage of polarization ranging from 0 to 100%. Interested readers may wish to refer to Section 6.6 for further details on this subject.

The theory of Rayleigh scattering developed in Section 3.3.1 is based on the assumption that molecules are homogeneous and isotropic spheres. However, molecules are in general anisotropic, whereby their polarizability, as defined in Eq. (3.3.16), varies along three axes and, hence, is a tensor instead of a scalar. The anisotropic effect of molecules reduces the degree of linear polarization defined in Eq. (3.3.22) by only a small percentage. At the 90° scattering angle, the degree of linear polarization for dry air is about 0.94. Further, the theory of Rayleigh scattering developed previously considers only single (or primary) scattering, i.e., where scattering occurs only once. But in the earth's atmosphere, which contains a large number of molecules and aerosol particles, light may undergo an infinite number of scattering events. In addition, the earth's surface also reflects light that reaches it. Multiple scattering processes involving the atmosphere and the surface become complicated and require a more advanced treatment of radiative transfer theory, which will be discussed in Chapter 6.

The theory of Rayleigh scattering predicts *neutral points,* i.e., points of zero polarization, only at the exact forward and backward directions. However, owing to multiple scattering of molecules and particulates, and reflection of the surface, there normally exist a number of neutral points in cloudless atmospheres. The first observations of neutral points and partially polarized sky light were made by Arago in

1809. He discovered the existence of a neutral point at a position in the sky about 25° above the antisolar direction (the direction exactly opposite that of the sun). The other two neutral points, which normally occur in the sunlit sky 25° above and 20° below the sun, were discovered by Babinet in 1840 and by Brewster in 1842, respectively. These three neutral points were named to honor these three discoverers. The neutral points in the sky vary and depend on the turbidity (an indication of the amount of aerosol loadings in the atmosphere), the sun's elevation angle, and the reflection characteristics of the surface at which observations are made.

Figure 3.12 illustrates the distribution of the degree of polarization and neutral points for a pristine, clear atmosphere (January 20, 1977) and for an atmospheric condition under the El Chichon volcanic cloud (July 27, 1982) observed at the Mauna Loa Observatory from a polarimeter developed by Coulson (1983). The observations
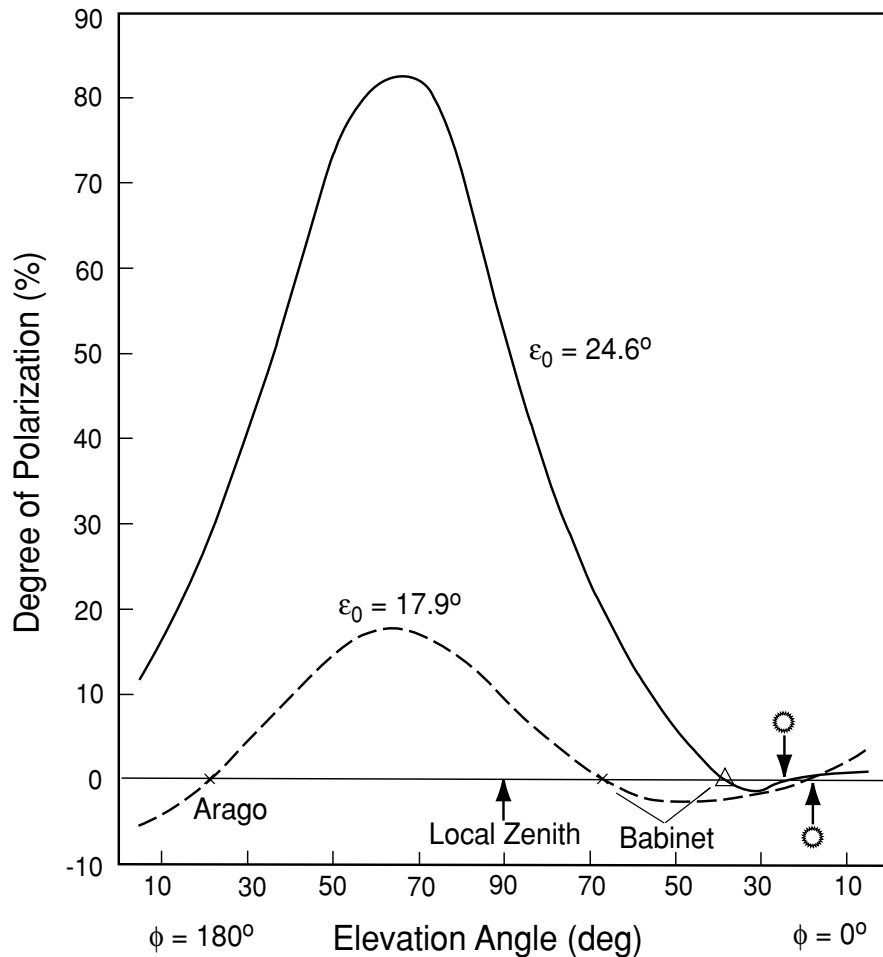


**Figure 3.12**   Illustration of neutral points in the distribution of the degree of polarization through the plane of the sun's vertical at a wavelength of 0.7 $\mu$m observed at the Mauna Loa Observatory for a clear atmospheric condition on January 20, 1977 (solid line), and for an atmosphere under the volcanic cloud on July 27, 1982 (dashed line). The azimuthal angles $\phi = 0°$ and $\phi = 180°$ are on the sun's vertical plane. The sun's elevation angles $\varepsilon_0$ for these two cases are indicated in the graph, as are the positions of Arago and Babinet (data taken from Coulson, 1983).

were made on the sun's vertical plane, referred to as the principal plane in radiative transfer, using a wavelength of $0.7\,\mu$m. The solar elevation angle, $\varepsilon_0$ ($90° -$ solar zenith angle $\theta_0$), differed slightly on these two dates, but the observed polarization patterns suffice to demonstrate their substantial variabilities in clear and turbid atmospheres. The clear Rayleigh atmosphere produced a maximum polarization of about $80\%$, $60\%$ more than that generated in the volcanic cloud condition. The neutral points in the Rayleigh scattering atmosphere occurred at the positions close to the sun (forward direction) and about $20°$ above the sun, the Babinet point, which was about $50°$ above the sun when a significant aerosol loading was present. In this case, the Arago point was also shown at about $20°$ above the horizon at the opposite position of the sun. Because of the sun's position, the Brewster point was not observed. The neutral points' positions are dependent on the aerosol optical depth and composition. Thus, a systematic observation of these points could be a valuable approach for inferring aerosol optical properties and perhaps composition information.

## 3.3.2   Light Scattering by Particulates: Approximations

In Section 1.1.4, we defined the size parameter, $x = 2\pi a/\lambda$, where $a$ is the particle radius. Rayleigh scattering is concerned with scattering events when $x \ll 1$. When $x \gtrsim 1$, scattering events are often called *Lorenz–Mie scattering*. Lorenz (1890) and Mie (1908) independently derived the solution for the interaction of a plane wave with an isotropic homogenous sphere. The mathematical theory of Lorenz–Mie scattering begins with Maxwell's equations and will be detailed in Chapter 5, along with some new developments in research on light scattering by nonspherical ice crystals and aerosols. In this section, however, we shall present a brief discussion of Lorenz–Mie scattering and two elementary approximations: geometric optics and anomalous diffraction.

### 3.3.2.1   LORENZ–MIE SCATTERING

The intensity scattered by a particle as a function of direction, as presented in Eq. (3.3.15), is given by

$$I(\Theta) = I_0 \Omega_{\text{eff}} \frac{P(\Theta)}{4\pi} = I_0 \left(\frac{\sigma_s}{r^2}\right) \frac{P(\Theta)}{4\pi}, \qquad (3.3.23)$$

where $I_0$ is the incident intensity, $P$ is the phase function normalized according to Eq. (3.3.10), $\Omega_{\text{eff}}$ is the effective solid angle upon which scattering occurs, $r$ is the distance between the particle and the observer, $\sigma_s$ is the scattering cross section, and $4\pi$ is the solid angle for the entire spherical space. The scattering cross section can be derived from the Lorenz–Mie theory of light scattering by spheres and is given by the following expansion:

$$\sigma_s/\pi a^2 = Q_s = c_1 x^4 \left(1 + c_2 x^2 + c_3 x^4 + \cdots\right), \qquad (3.3.24)$$

where $a$ is the radius, $x = 2\pi a/\lambda$, $Q_s$ is referred to as the *scattering efficiency,* and the coefficients in the case of nonabsorbing particles are given by

$$c_1 = \frac{8}{3}\left(\frac{m^2-1}{m^2+2}\right)^2, \quad c_2 = \frac{6}{5}\left(\frac{m^2-1}{m^2+2}\right),$$

$$c_3 = \frac{3}{175}\frac{m^6+41m^4-28m^2+284}{(m^2+2)^2} + \frac{1}{900}\left(\frac{m^2+2}{2m^2+2}\right)^2\left[15+(2m^2+3)^2\right].$$

The leading term is the dipole mode contribution associated with Rayleigh scattering. Note that for light scattering by spheres, we may replace the total number of molecules per volume $N_s$ by $1/V$ where $V = 4\pi a^3/3$. For molecules, $a \sim 10^{-4}$ $\mu$m, so that $x \sim 10^{-3}$ in the visible. Thus, the higher order terms can be neglected and the scattered intensity is proportional to $\lambda^{-4}$. For aerosols and cloud particles, $a \gtrsim 10^{-1}$ $\mu$m, and $x \gtrsim 1$ in the visible. In this case, the scattered intensity is less wavelength dependent and is primarily dependent on particle size. As a result, clouds and nonabsorbing aerosols in the atmosphere generally appear white. In a cloudy atmosphere, the sky appears blue diluted with white scattered light, resulting in a less pure blue sky than would have been expected from pure Rayleigh scattering.

On the basis of Eq. (3.3.23), the scattered intensity is dependent on the phase function, which can be computed from the Lorenz–Mie theory for spheres. Figure 3.13 shows typical examples of the phase function for polydispersed cloud droplets ($\sim$10 $\mu$m) and aerosols ($\sim$1 $\mu$m) illuminated by a visible light. Also shown is the phase function for Rayleigh scattering. The mean size parameters in these cases are about 100, 10, and $10^{-3}$, respectively. The scattering by cloud droplets is characterized by a strong forward diffraction; a minimum at $\sim$100° scattering angle; a peak at $\sim$138° scattering angle, the well-known rainbow feature; and a peak in the backscattering direction associated with the glory pattern. The diffraction pattern and the rainbow feature will be discussed further later; the explanation of the glory pattern requires more advanced discussion and will be presented in Chapter 5. The scattering of typical aerosols also displays a forward diffraction maximum and a maximum pattern in the 150°–170° scattering region (see also Fig. 1.4).

### 3.3.2.2 GEOMETRIC OPTICS

The principles of geometric optics are the asymptotic approximations of the fundamental electromagnetic theory and are valid for light-scattering computations involving a particle whose dimension is much larger than the wavelength, i.e., $x \gg 1$. In this case, a light beam can be thought of as consisting of a bundle of separate parallel rays that hit the particles, which is referred to as the *localization principle*. Each ray will then undergo reflection and refraction and will pursue its own path along a straight line outside and inside the scatterer with propagation directions determined by the *Snell law,* as shown in Fig. 3.14a. In the context of geometric optics, the total electric field is assumed to consist of the diffracted rays and the reflected and refracted rays, as illustrated in Fig. 3.14b, using a sphere as an example. The diffracted rays
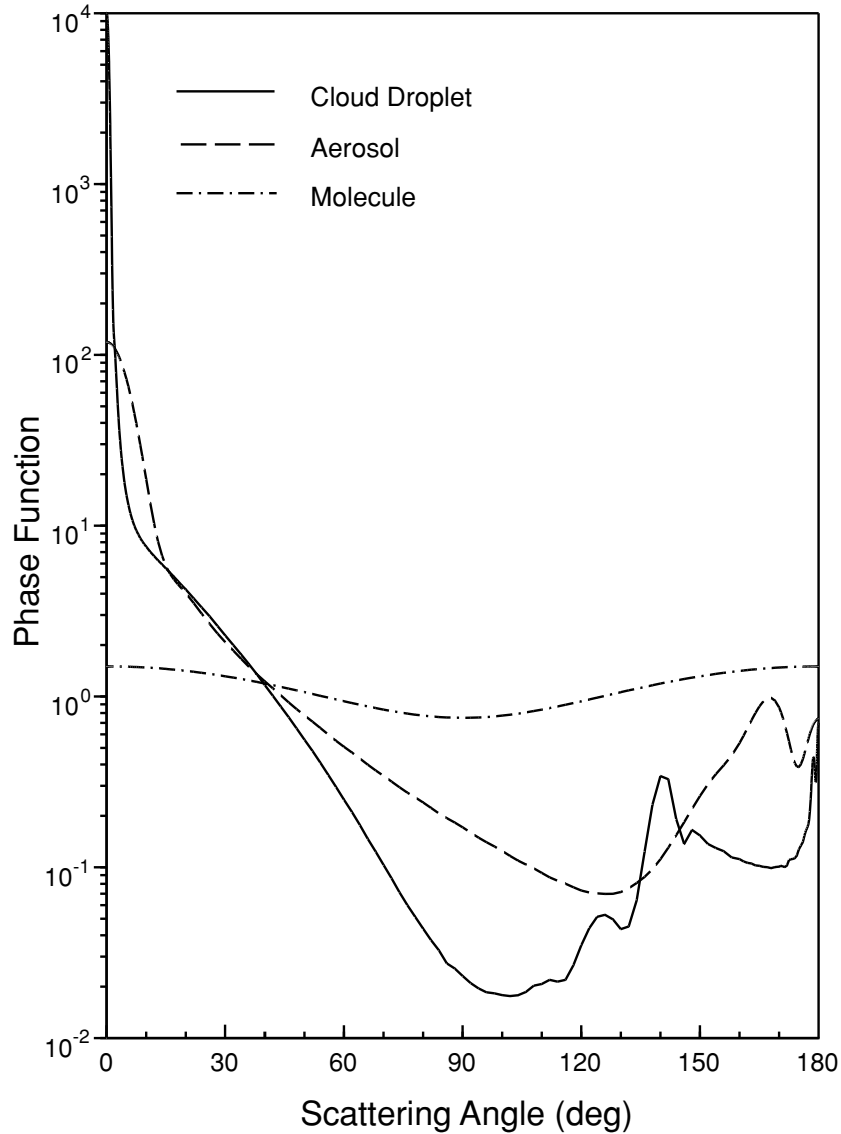
**Figure 3.13**   Normalized phase functions for cloud droplets ($\sim 10$ $\mu$m), aerosols ($\sim 1$ $\mu$m), and molecules ($\sim 10^{-4}$ $\mu$m) illuminated by a visible wavelength of 0.5 $\mu$m, computed from the Lorenz–Mie theory.

pass around the scatterer. The rays impinging on the scatterer undergo local reflection and refraction, referred to as *Fresnelian interaction*. The energy that is carried by the diffracted and the Fresnelian rays is assumed to be the same as the energy that is intercepted by the particle cross section projected along the incident direction.

In reference to Fig. 3.14a, let $v_1$ and $v_2$ be the velocities of propagation of plane waves in the two media such that $v_1 > v_2$. Also, let $\theta_i$ and $\theta_t$ be the angles corresponding to the incident and refracted waves. Thus, we have

$$\sin \theta_i / \sin \theta_t = v_1/v_2 = m, \tag{3.3.25}$$

where $m$ is the index of refraction for the second medium with respect to the first.

(a)

Normal of Incidence

Incident Wave

Reflected Wave

$\theta_i$   $\theta_r$

Air

Water/Ice

$\theta_t$

Refracted Wave

(b)

Light rays

1   4

2

0

3
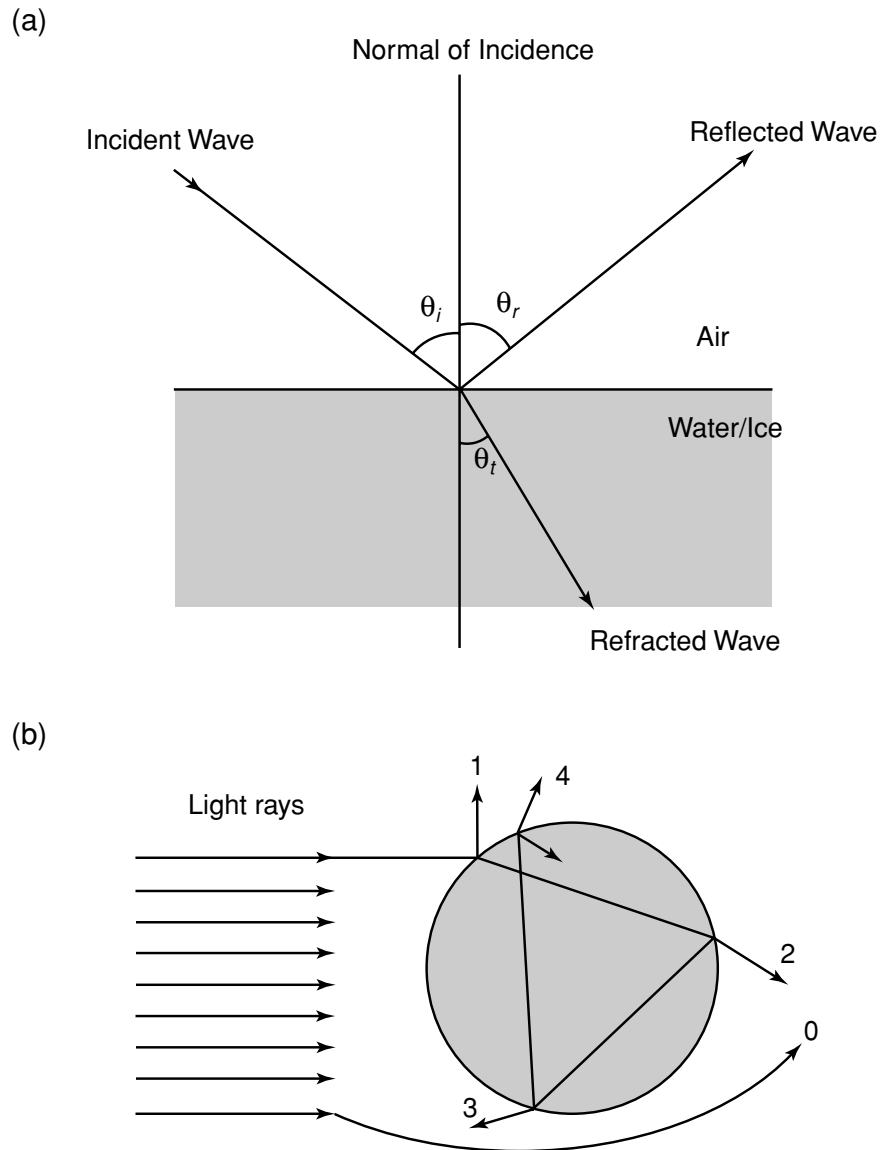
**Figure 3.14**   (a) Reflection and refraction of a plane wave from air to water/ice surface. (b) Representation of light rays scattered by a sphere based on the geometric optics principle: 0, exterior diffraction; 1, external reflection; 2, two refractions; 3, one internal reflection; and 4, two internal reflections.

For the purpose of this discussion, we shall assume that there is no absorption in the medium. This is the *Snell law* relating the incident and refracted angles through the index of refraction. Exercises 3.12 and 3.13 require the derivation of the minimum deviations of light rays that produce *rainbows* from spherical water droplets and *halos* from hexagonal ice crystals. Moreover, white sunlight is decomposed into component colors after the rays undergo geometric reflection and refraction through water droplets and ice crystals.

The diffraction component in geometric optics can be determined from *Babinet's principle*. This principle states that the diffraction pattern in the far field, referred to as *Fraunhofer diffraction,* from a circular aperture is the same as that from an opaque

disk or sphere of the same radius. Based on this principle and geometric consideration, the scattered intensity is proportional to

$$I_p = \frac{x^4}{4} \left[ \frac{2 J_1(x \sin \Theta)}{x \sin \Theta} \right]^2 , \qquad (3.3.26)$$

where $J_1$ is the first-order *Bessel function* and $\Theta$ is the scattering angle. Exercise 3.14 requires the calculation of maxima and minima of the diffraction pattern that can be used to explain an optical phenomenon known as the *corona*.

One final note is in order here. If a particle of any shape is much larger than the incident wavelength, the total energy removed is based on geometric reflection and refraction, giving an effective cross-section area equal to the geometric area $A$. In addition, according to Babinet's principle, diffraction takes place through a hole in this area, giving a cross-section area also equal to $A$. The total removal of incident energy is therefore twice the geometric area. Thus, the extinction cross section is given by

$$\sigma_e = 2A, \text{ or } Q_e = \sigma_e/A = 2, \qquad (3.3.27)$$

where $Q_e$ is called the *extinction efficiency*. This is referred to as the *optical theorem of extinction*. If a particle is nonabsorbing, then we have $Q_e = Q_s$, where the extinction and scattering efficiencies are the same.

### 3.3.2.3   ANOMALOUS DIFFRACTION THEORY

Consider large optically soft particles such that $x \gg 1$ and $|m - 1| \ll 1$. The second condition implies that rays are negligibly deviated as they cross the soft particle boundary and are negligibly reflected because the refractive indices inside and outside the particle are similar. In this case, the extinction is largely caused by absorption of the light beam passing through the particle, as well as by the interference of light passing through the particle and passing around the particle. This is the physical foundation for the anomalous diffraction theory originally developed by van de Hulst (1957). In reference to Fig. 3.15, let the plane wave be incident on a spherical particle with a radius $a$ and a refractive index $m \to 1$. The wave front on the forward side of the particle can be divided into two types: one within the geometric shadow area denoted by $A = \pi a^2$, and one outside this area denoted by $B$. The incident rays can undergo diffraction and pass around the particle. The rays can also hit the particle and undergo reflection and refraction. Since $m \to 1$, we may assume that the rays enter into the particle and pass through it, as illustrated in Fig. 3.15. However, these rays will have phase lags due to the presence of the particle. The phase lag for the ray indicated in the figure is $2a \sin \alpha (m - 1) \cdot 2\pi/\lambda$. If we define the phase shift parameter

$$\rho = 2x(m - 1), \qquad (3.3.28)$$

the phase lag can then be expressed by $\rho \sin \alpha$.

Consider a screen that collects the field. The resultant wave on the screen is the sum of the incident and scattered fields. If the incident field is assumed to be unity,

Incident Rays

$\pi a^2$

$m \longrightarrow 1$

$a$

$\alpha$

$d\alpha$

$dA$
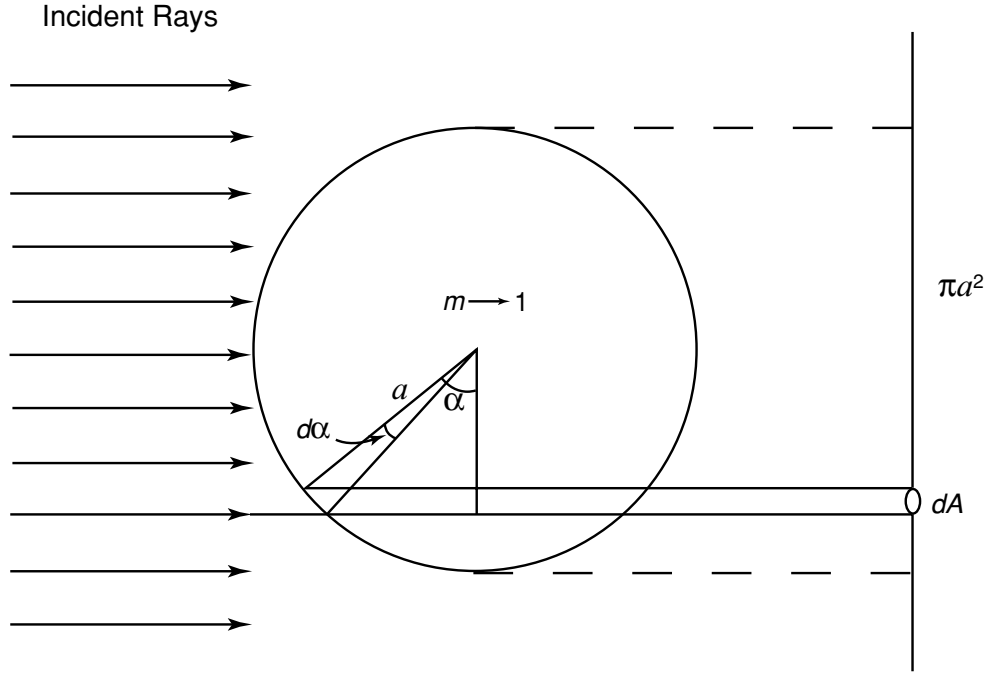
**Figure 3.15** Geometry of anomalous diffraction through a sphere with a radius $a$ and an index of refraction $m \to 1$. $\pi a^2$ denotes the geometric cross-section area of the sphere and $dA$ denotes the differential cross-section area.

then in the forward direction ($\Theta = 0$), the change in the electric field is proportional to

$$A = \int \int \left(1 - e^{-i\rho \sin \alpha}\right) dx\, dy. \tag{3.3.29a}$$

The differential area can be replaced by an area in the polar coordinate such that $dx\, dy = a \cos \alpha \, d(a \cos \alpha) \, d\phi$. Thus, we have

$$A = \int_0^{2\pi} \int_0^{\pi/2} \left(1 - e^{-i\rho \sin \alpha}\right) a^2 \sin \alpha \, d \sin \alpha \, d\phi = 2\pi a^2 K(i\rho), \tag{3.3.29b}$$

where

$$K(i\rho) = \frac{1}{2} + \frac{e^{-i\rho}}{i\rho} + \frac{e^{-i\rho} - 1}{(i\rho)^2}. \tag{3.3.30}$$

The extinction cross section $\sigma_e$ is proportional to the differential change in the scattered intensity $I$. Since $I \sim |E|^2$, as shown in Eq. (3.3.6), $dI \sim 2d|E|$. Thus, we have $\sigma_e = 2\mathrm{Re}(A)$. It follows that the extinction efficiency is given by

$$Q_e = \sigma_e/\pi a^2 = 4\mathrm{Re}[K(i\rho)] = 2 - \frac{4}{\rho} \sin \rho + \frac{4}{\rho^2}(1 - \cos \rho), \tag{3.3.31}$$

where Re denotes the real part of the function. Exercise 3.15 requires calculations of $Q_e$.

We may also determine the absorption efficiency by the following procedure. The ray path as shown in Fig. 3.15 is $l = 2a \sin \alpha$. The absorption coefficient $k_i = m_i 2\pi/\lambda$,

where $m_i$ is the imaginary part of the refractive index. Thus, the absorption path length associated with the electric field is $lk_i$. The attenuation of the intensity of the ray is then $\exp(-2lk_i)$ and the absorption cross section for all possible rays is

$$\sigma_a = \int \int \left(1 - e^{-2lk_i}\right) dx\, dy. \tag{3.3.32}$$

Following the procedure just illustrated, the absorption efficiency is given by

$$Q_a = \sigma_a/\pi a^2 = 1 + \frac{2}{b}e^{-b} + \frac{2}{b^2}(e^{-b} - 1), \tag{3.3.33}$$

where $b = 4xm_i$ and $x = 2\pi a/\lambda$. The approximation based on the anomalous diffraction theory (ADT) is useful for the calculation of the extinction and absorption coefficients when $m \to 1$. It can also be applied to nonspherical particles such as spheroids and hexagons. Since refractions and reflections of rays are neglected in this approximation, its accuracy must be examined carefully when applied to the scattering of ice crystals ($m \sim 1.31$) and aerosols ($m \sim 1.5$). Finally, it should be noted that the ADT approximation cannot produce the phase function pattern.

## 3.4   Multiple Scattering and Absorption in Planetary Atmospheres

### 3.4.1   Fundamentals of Radiative Transfer

In Section 1.1.4, we pointed out that scattering is often coupled with absorption. In the following we formulate the fundamental equation governing the transfer of diffuse solar radiation in plane-parallel atmospheres. The term *diffuse* is associated with multiple scattering processes and is differentiated from *direct* solar radiation. In reference to Fig. 3.16 and considering a differential thickness $\Delta z$, the differential change of diffuse intensity emergent from below the layer is due to the following processes: (1) reduction from the extinction attenuation; (2) increase from the single scattering of the unscattered direct solar flux from the direction $(-\mu_0, \phi_0)$ to $(\mu, \phi)$; (3) increase from multiple scattering of the diffuse intensity from directions $(\mu', \phi')$ to $(\mu, \phi)$; and (4) increase from emission within the layer in the direction $(\mu, \phi)$. Consider a small volume containing a spectrum of molecules and/or particulates and denote the extinction, scattering, and absorption coefficients (in units of per length) as $\beta_e$, $\beta_s$, and $\beta_a$, respectively, defined by

$$\beta_{e,s,a} = \int_{\Delta z} \sigma_{e,s,a}(z)n(z)\, dz/\Delta z, \tag{3.4.1}$$

where the symbol $\sigma$ denotes the cross section and $n$ is the number density. Moreover, let the phase function corresponding to a volume of particulates be $P$. Thus, $P(\mu, \phi; \mu', \phi')$ denotes the redirection of the incoming intensity defined by $(\mu', \phi')$ to the outgoing intensity defined by $(\mu, \phi)$. Also note that the differential length
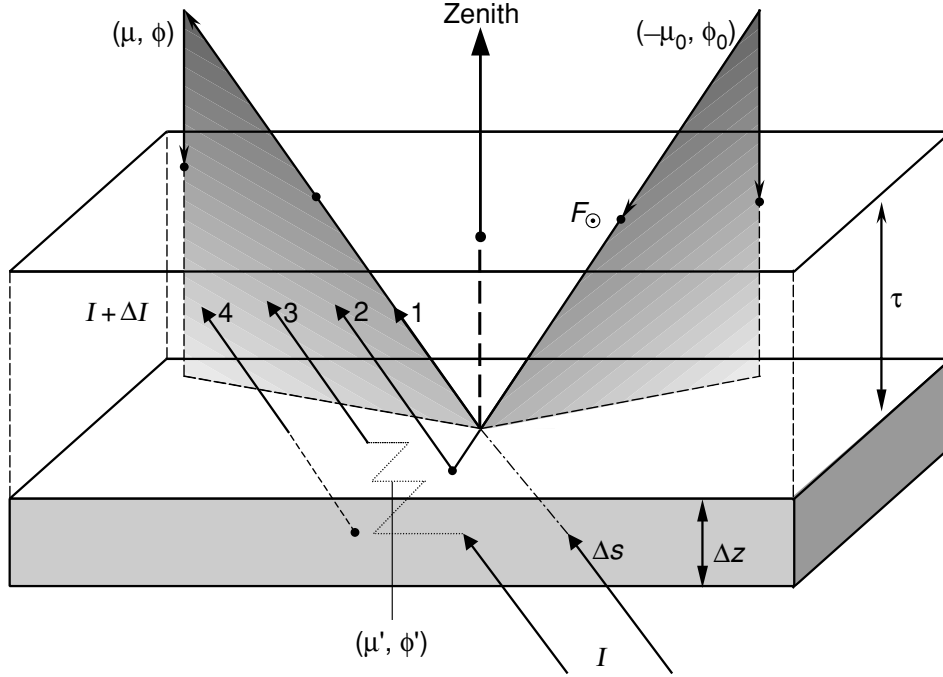
**Figure 3.16**   Transfer of diffuse solar intensity from below in plane-parallel layers: (1) attenuation by extinction; (2) single scattering of the unscattered solar flux; (3) multiple scattering; and (4) emission from the layer. All the radiative parameters are defined with reference to a small volume containing a spectrum of molecules and/or particulates. The notations are defined in the text.

$\Delta s = \Delta z / \mu$. Based on the preceding definitions, we may write (neglecting the wavelength index)

$$\frac{\Delta I(z; \mu, \phi)}{\Delta z / \mu} = -\beta_e I(z; \mu, \phi) + \beta_s F_\odot e^{-\tau/\mu} \cdot P(\mu, \phi; -\mu_0, \phi_0)/4\pi$$

$$+\beta_s \int_0^{2\pi} \int_{-1}^{1} I(z, \mu', \phi') \cdot P(\mu, \phi; \mu', \phi')/4\pi \, d\mu' d\phi' + \beta_a B[T(z)].$$

$$(3.4.2)$$

All the terms are self-explanatory. However, it is noted that integration of the multiple scattering term is performed for diffuse intensity over the $4\pi$ solid angle and that radiative equilibrium is assumed such that emission is equal to absorption based on Kirchhoff's and Planck's laws (Section 1.2).

Further, we may define the single-scattering albedo as the ratio of the scattering coefficient to the extinction coefficient in the form

$$\tilde{\omega} = \frac{\beta_s}{\beta_e} \quad \text{or} \quad 1 - \tilde{\omega} = \frac{\beta_a}{\beta_e}. \qquad (3.4.3)$$

The optical depth is defined by

$$\tau = \int_z^\infty \beta_e \, dz'. \qquad (3.4.4)$$

Using the optical depth, Eq. (3.4.2) can be rewritten as follows:

$$\mu\frac{dI(\tau;\mu,\phi)}{d\tau} = I(\tau;\mu,\phi) - J(\tau;\mu,\phi), \tag{3.4.5}$$

where the source function is given by [see also Eq. (1.4.22)]

$$J(\tau;\mu,\phi) = \frac{\tilde{\omega}}{4\pi}\int_0^{2\pi}\int_{-1}^{1} I(\tau;\mu',\phi')P(\mu,\phi;\mu',\phi')d\mu'd\phi'$$

$$+ \frac{\tilde{\omega}}{4\pi}F_\odot P(\mu,\phi;-\mu_0,\phi_0)e^{-\tau/\mu_0} + (1-\tilde{\omega})B[T(\tau)]. \tag{3.4.6}$$

The fundamental parameters that drive the transfer of diffuse intensity are the extinction coefficient (or the optical depth), the single-scattering albedo, and the phase function. It suffices to assume that these parameters are independent of $\tau$ (or $z$) in the present discussion. Interested readers should refer to Chapter 6 for an in-depth explanation of radiative transfer processes. For discussion of solar radiative transfer, the flux emitted from the earth and the atmosphere with an equilibrium temperature of $\sim$255 K is negligible in comparison to that emitted from the sun for $\lambda \le 3.5\ \mu$m. For some solar radiative transfer problems, we may then omit the last term in the source function.

　　The phase function represents the angular distribution of the scattered energy as a function of the scattering angle and has been presented for molecules, aerosols, and cloud particles in Fig. 3.13. From spherical geometry, the scattering angle is related to the incoming and outgoing directions in the form

$$\cos\Theta = \mu\mu' + (1-\mu^2)^{1/2}(1-\mu'^2)^{1/2}\cos(\phi'-\phi). \tag{3.4.7}$$

We may express the phase function in terms of a known mathematical function for the purpose of solving Eq. (3.4.5), the first-order differential integral equation. The Legendre polynomials (Appendix E), by virtue of their unique mathematical properties, have been used extensively in the analysis of radiative transfer problems. In terms of Legendre polynomials $P_\ell$, the phase function may be written in the form

$$P(\cos\Theta) = \sum_{\ell=0}^{N}\tilde{\omega}_\ell P_\ell(\cos\Theta), \tag{3.4.8}$$

where the expansion coefficient, based on the orthogonal property, is given by

$$\tilde{\omega}_\ell = \frac{2\ell+1}{2}\int_{-1}^{1} P(\cos\Theta)P_\ell(\cos\Theta)\,d\cos\Theta, \quad \ell = 0, 1\dots, N. \tag{3.4.9a}$$

When $\ell = 0$, $\tilde{\omega}_0 = 1$, representing the normalization of the phase function denoted in Eq. (3.3.10). When $\ell = 1$, we have

$$g = \frac{\tilde{\omega}_1}{3} = \frac{1}{2}\int_{-1}^{1} P(\cos\Theta)\cos\Theta\,d\cos\Theta. \tag{3.4.9b}$$

This term is referred to as the *asymmetry factor,* which is the first moment of the phase function and an important parameter in radiative transfer. For isotropic scattering, $g$ is

zero, as it is for Rayleigh scattering (Exercise 3.16). The asymmetry factor increases as the diffraction peak of the phase function sharpens and can be negative if the phase function peaks in backward directions (90–180°). For Lorenz–Mie type particles, whose phase function has a generally sharp peak at the 0° scattering angle (Fig. 3.13), the asymmetry factor denotes the relative strength of forward scattering.

## 3.4.2  Approximations of Radiative Transfer

We shall present two useful approximations: one for remote sensing applications, and the other for radiation parameterization for use in climate studies.

### 3.4.2.1  SINGLE-SCATTERING APPROXIMATION

In a domain where the optical depth is small (e.g., $\tau < 0.1$), a large portion of scattering events is dominated by single scattering of the direct solar beam. This occurs in optically thin cirrus and aerosol atmospheres. In this case, the most important term in the source function is

$$J(\tau; \mu, \phi) \cong \frac{\tilde{\omega}}{4\pi} F_\odot P(\mu, \phi; -\mu_0, \phi_0)e^{-\tau/\mu_0}. \qquad (3.4.10)$$

Consider a black surface such that the reflected upward intensity $I(\tau_*; \mu, \phi) = 0$, where $\tau_*$ is the total atmospheric optical depth. From Eq. (1.4.23), the upward intensity at the top of the atmosphere is

$$I(0; \mu, \phi) = \int_0^{\tau_*} J(\tau'; \mu, \phi)e^{-\tau'/\mu}\frac{d\tau'}{\mu}$$

$$= \frac{\mu_0 F_\odot}{\pi}\frac{\tilde{\omega}}{4(\mu + \mu_0)}P(\mu, \phi; -\mu_0, \phi_0)\left\{1 - \exp\left[-\tau_*\left(\frac{1}{\mu} + \frac{1}{\mu_0}\right)\right]\right\}.$$

$$(3.4.11a)$$

Moreover, for a small $\tau_*$, we have

$$R(\mu, \phi; \mu_0, \phi_0) = \frac{\pi I(0; \mu, \phi)}{\mu_0 F_\odot} = \tau_*\frac{\tilde{\omega}}{4\mu\mu_0}P(\mu, \phi; -\mu_0, \phi_0). \quad (3.4.11b)$$

The term $R$ is a nondimensional quantity, referred to as the *bidirectional reflectance*. This equation establishes the foundation for the retrieval of the optical depth of aerosols from satellites. It is clear that under the condition of optically thin atmosphere, the optical depth is directly proportional to the bidirectional reflectance that can be determined from satellite radiometric measurements, but is inversely proportional to the phase function. The latter dependence becomes an important issue in satellite remote sensing using reflected sunlight, a subject that will be discussed further in Section 7.3.1.

### 3.4.2.2   DIFFUSION APPROXIMATION

Consider a diffusion domain where the directional dependence of multiple scattering events is largely lost. In this case, it is appropriate to consider the transfer of hemispheric upward and downward flux densities defined by [see also Eq. (1.1.9)]

$$F^{\uparrow\downarrow}(\tau) = \int_0^{2\pi} \int_0^{\pm 1} I(\tau; \mu, \phi)\mu\, d\mu\, d\phi, \qquad (3.4.12)$$

where the notations $\uparrow$ and $\downarrow$ correspond to $+$ and $-$, respectively. We may formulate the transfer problem based on the physical reasoning that the differential changes of the upward and downward flux densities must be related to these fluxes as well as to the direct downward flux from the sun. Thus, we write,

$$\frac{dF^{\uparrow}}{d\tau} = \gamma_1 F^{\uparrow} - \gamma_2 F^{\downarrow} - \gamma_3 \tilde{\omega} F_{\odot} e^{-\tau/\mu_0}, \qquad (3.4.13a)$$

$$\frac{dF^{\downarrow}}{d\tau} = \gamma_2 F^{\uparrow} - \gamma_1 F^{\downarrow} + (1 - \gamma_3)\tilde{\omega} F_{\odot} e^{-\tau/\mu_0}, \qquad (3.4.13b)$$

where $\gamma_1, \gamma_2$, and $\gamma_3$ are appropriate weighting coefficients related to multiple scattering events. The two flux equations were first formulated by Schuster (1905), although in a slightly different format. These equations can be derived from the well-known two-stream and Eddington approximations in which the three coefficients can be determined (see Chapter 6). Solutions for the upward and downward fluxes can be derived by setting $F_{\text{dif}} = F^{\downarrow} - F^{\uparrow}$, and $F_{\text{sum}} = F^{\downarrow} + F^{\uparrow}$. In this manner we can show that (Exercises 3.17 and 3.18)

$$\frac{d^2 F_{\text{dif}}}{d\tau^2} = k^2 F_{\text{dif}} + \chi e^{-\tau/\mu_0}, \qquad (3.4.14)$$

where $k^2 = \gamma_1^2 - \gamma_2^2$ are the eigenvalues and $\chi$ is a certain coefficient. Equation (3.4.14) is referred to as the *diffusion equation for radiative transfer*. The general solution for this second-order nonhomogeneous differential equation is given by

$$F_{\text{dif}} = c_1 e^{-k\tau} + c_2 e^{+k\tau} + \chi(1/\mu_0^2 - k^2)e^{-\tau/\mu_0}, \qquad (3.4.15)$$

where $c_{1,2}$ are certain coefficients. Likewise, we can also derive a solution for $F_{\text{sum}}$ which, together with $F_{\text{dif}}$, can be used to determine the analytic solutions for upward and downward flux densities. Interested readers should consult Section 6.5.2 for an advanced discussion of this topic.

Many general circulation and climate models utilize the two-stream or Eddington's approximation in the parameterization of radiative transfer because analytic solutions can be derived to achieve efficient computation that is critical for model simulations. In the following, the subject of atmospheric absorption in multiple scattering atmospheres that leads to the production of solar heating rates is further discussed.

## 3.5    Atmospheric Solar Heating Rates

The absorption of solar radiation by various gases is important because of its generation of heating in the atmosphere, which is also affected by multiple scattering processes. Consider a plane-parallel absorbing and scattering atmosphere illuminated by the solar spectral irradiance $F_\odot$ so that the downward flux density normal to the top of the atmosphere is given by $\mu_0 F_\odot$. Let the differential thickness within the atmosphere be $\Delta z$, and let the spectral downward and upward flux densities centered at wavelength $\lambda$ be denoted by $F^\downarrow$ and $F^\uparrow$, respectively. We have omitted the wavelength dependence for simplicity of presentation. The net flux density (downward) at a given height $z$ is then defined by

$$F(z) = F^\downarrow(z) - F^\uparrow(z). \qquad (3.5.1a)$$

In reference to Fig. 3.17, because of absorption, the net flux density decreases from the upper levels to the progressively lower levels. The loss of net flux density, i.e., the
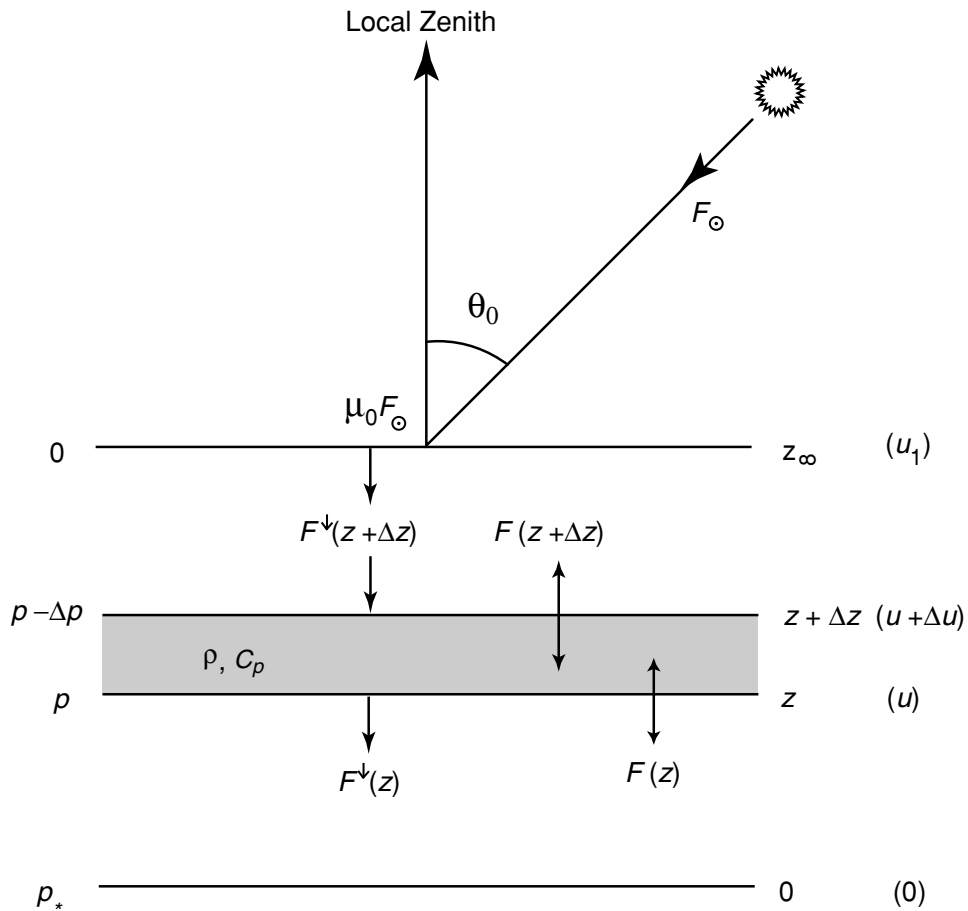


**Figure 3.17**    Divergence of the net flux density in $z$, $p$, and $u$ coordinates. All the notations are defined in the text.

net flux density divergence for the differential layer is, therefore,

$$\Delta F(z) = F(z) - F(z + \Delta z). \tag{3.5.1b}$$

On the basis of the energy conservation principle, the absorbed radiant energy must be used to heat the layer. Thus, the heating experienced by a layer of air due to radiation transfer may be expressed in terms of the rate of temperature change. It is conventionally given by

$$\Delta F(z) = -\rho C_p \Delta z \frac{\partial T}{\partial t}, \tag{3.5.2}$$

where $\rho$ is the air density in the layer, $C_p$ is the specific heat at constant pressure, and $t$ is the time. The heating rate for a differential layer $\Delta z$ is, therefore,

$$\frac{\partial T}{\partial t} = -\frac{1}{\rho C_p} \frac{\Delta F(z)}{\Delta z} = \frac{g}{C_p} \frac{\Delta F(p)}{\Delta p} = -\frac{q}{C_p} \frac{\Delta F(u)}{\Delta u}, \tag{3.5.3}$$

where we have also expressed the heating rate in terms of pressure and path-length coordinates using the hydrostatic equation $dp = -\rho g \, dz$, and the definition of path length for a specific gas where $q$ is the mixing ratio, $g$ is the gravitational acceleration, and $g/C_p$ is the well-known dry adiabatic lapse rate. If we divide the solar spectrum into $N$ intervals and carry out the heating rate calculations for each spectral interval $i$, then the total heating rate due to solar radiation may be written in the form

$$\left(\frac{\partial T}{\partial t}\right)_s = \sum_{i=1}^{N} \left(\frac{\partial T}{\partial t}\right)_i. \tag{3.5.4}$$

Computation of the solar flux and heating rate in the atmosphere covering the entire solar spectrum is quite involved. In a clear atmosphere, we must include both absorption by various absorbing gases, chiefly $H_2O$, $O_3$, $O_2$, and $CO_2$, and scattering by molecules and aerosols, as well as reflection from the surface. The solar spectrum must be divided into a number of suitably grouped subspectral intervals in which a monochromatic radiative transfer program, such as the adding or discrete-ordinates method for inhomogeneous atmospheres discussed in Chapter 6, can be employed for the calculation of spectral fluxes and heating rates. The single-scattering properties of each subdivided interval for input into the radiative transfer model must include simultaneous contributions from the scattering and absorption of aerosols (and cloud particles), Rayleigh scattering, and gaseous absorption. For efficient spectral integration, we may employ the correlated $k$-distribution method introduced in Section 4.3.

In Fig. 3.18, we show typical solar heating rates and net flux profiles as functions of the cosine of the solar zenith angle $\mu_0$ using the standard atmospheric profiles for $H_2O$, $O_3$, and other trace gases (see Fig. 3.2), along with a surface albedo of 0.1, as inputs of a radiative transfer model. The instantaneous solar heating rate profile is divided into two different levels to highlight the contributions from $H_2O$ and $O_3$. The solar heating rate decreases as $\mu_0$ decreases because the incoming solar irradiance available to the atmosphere is directly proportional to $\mu_0$. Below about 10 km, the solar heating rate is primarily produced by water vapor with the heating rate ranging
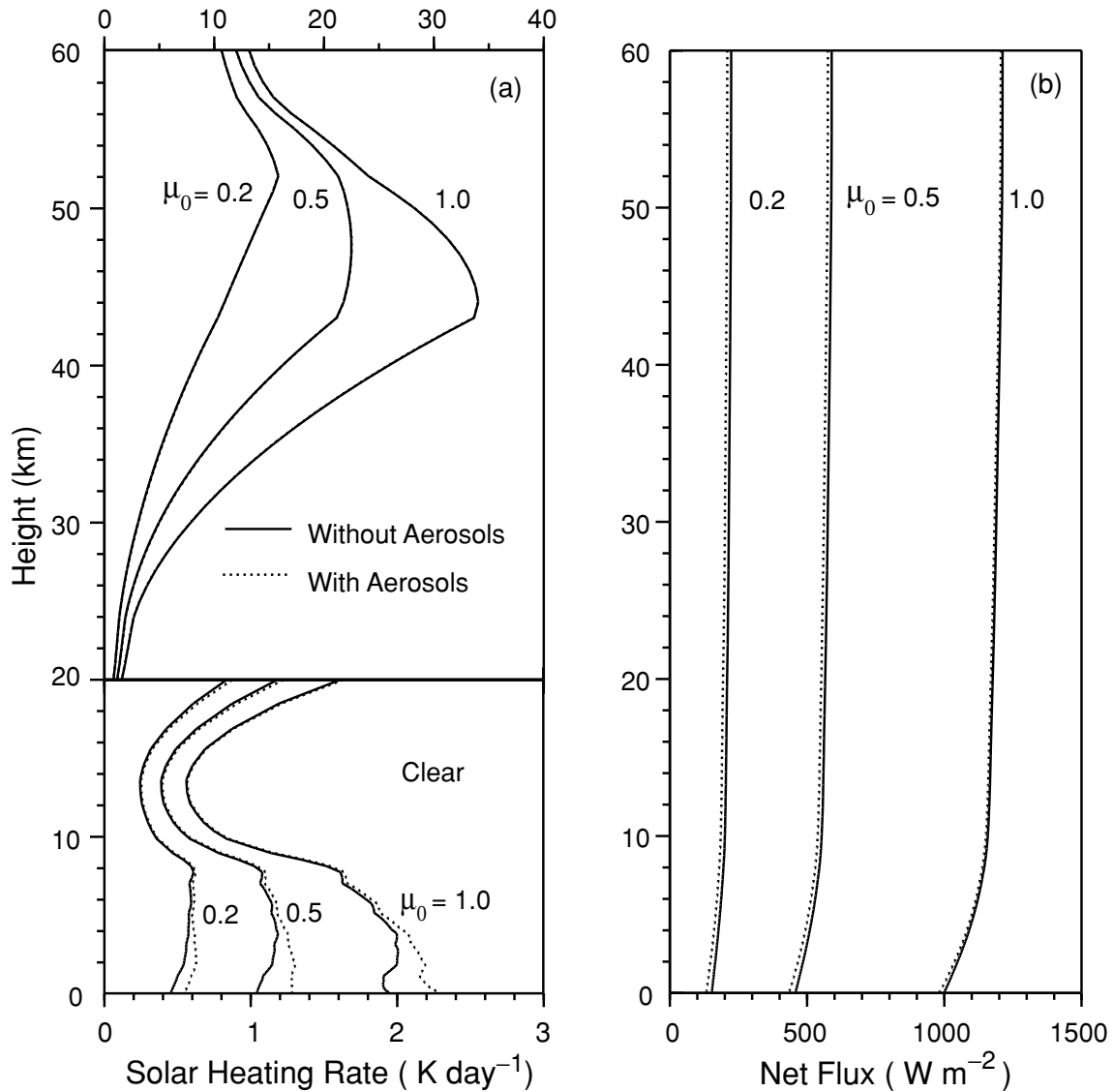
**Figure 3.18**  Solar heating rates and net fluxes as functions of height with and without the contribution of aerosols for a number of the cosines of solar zenith angles. The solar heating rates are instantaneous values and are separated in two regions to highlight the contributions from water vapor and ozone in the troposphere and stratosphere, respectively. A typical background aerosol profile with a visible optical depth of 0.15 is used to illustrate the effect of aerosols on the solar flux and heating rate. These results and those presented in Fig. 3.19 are computed from a line-by-line equivalent radiative transfer model that includes the contributions of gaseous absorption, multiple scattering, and the absorption of aerosol and cloud particles (Liou *et al.,* 1998).

from 0.5 to 2 $K\,day^{-1}$ near the surface when the contribution from aerosols is not accounted for. The solar heating rate decreases rapidly with increasing altitude in phase with the exponential decrease of water vapor and reaches a minimum at about 15 km. Above 20 km, increased solar heating is produced primarily by the absorption of ozone. Solar net flux decreases significantly below about 10 km. When a standard aerosol profile with an optical depth of 0.15 at the 0.5 $\mu$m wavelength is added, the solar heating rate increases in the lower atmosphere because of the absorption of aerosols in the visible and near infrared. The effect of aerosols on the absorption of
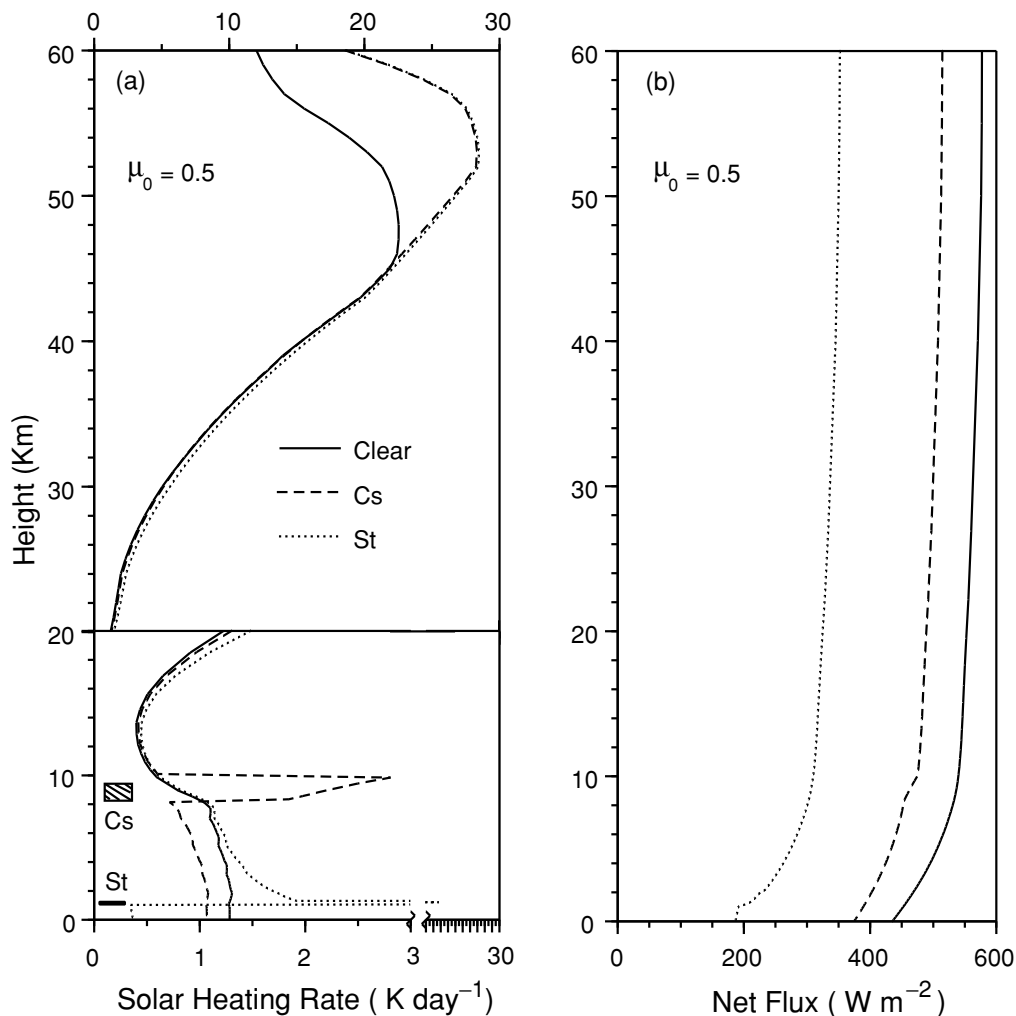
**Figure 3.19** Comparison of (a) solar heating rates and (b) net fluxes in clear, cirrus (Cs), and stratus (St) cloudy conditions for a $\mu_0$ of 0.5. The positions of these clouds are indicated in the diagram. The optical depths for Cs and St are 0.7 and 10, respectively, while the mean particle sizes are 42 and 8 $\mu$m, respectively.

solar fluxes depends on their chemical composition, particle size distribution, and vertical profile and is a subject of ongoing research.

The effects of clouds on solar heating and net flux profiles are investigated using typical single-layer cirrostratus (Cs) and stratus (St) clouds whose locations are shown in Fig. 3.19. We use a cosine of the solar zenith angle of 0.5 in this demonstration. The visible optical depths for Cs and St are 0.7 and 10, respectively, while the mean ice crystal maximum dimension and water droplet radius are 42 and 8 $\mu$m, respectively. In the case of low stratus, substantial instantaneous heating occurs at the cloud top with a value of about 22 K day$^{-1}$. Because of the reflection from clouds, ozone heating also increases. This increase appears to depend on the factors associated with cloud position and optical depth. In the overcast low stratus condition, net solar flux available at the surface is only about 187 W m$^{-2}$, in comparison to about 435 and 376 W m$^{-2}$ in clear and cirrus cloud conditions, respectively.

## Exercises

3.1  The scale height $H$ is defined by $dp/p = -dz/H$. From the hydrostatic equation and the equation of state, show that $H = KT/Mg$, where $K$ is the Boltzmann constant, $M$ is the molecular weight of air, and $g$ is gravity. Since the molecular translational energy is $\frac{1}{2}KT$, the scale height is then twice the distance through which atoms/molecules that have the equipartition of translational energy can rise in the vertical direction against the force of gravity.

3.2  Compute and display graphically $r(z_1)$ as a function of $z_1$, as defined in Eq. (3.2.6) for $\mu_0 = 1, 0.5$, and 0.2. Compare your results with those presented in Fig. 3.6 and explain the meaning of the Chapman layer.

3.3  In reference to the spherical atmosphere depicted in Fig. 3.20, derive the Chapman function $\text{Ch}(x, \theta_0)$. Compare this function with $1/\mu_0$ and determine
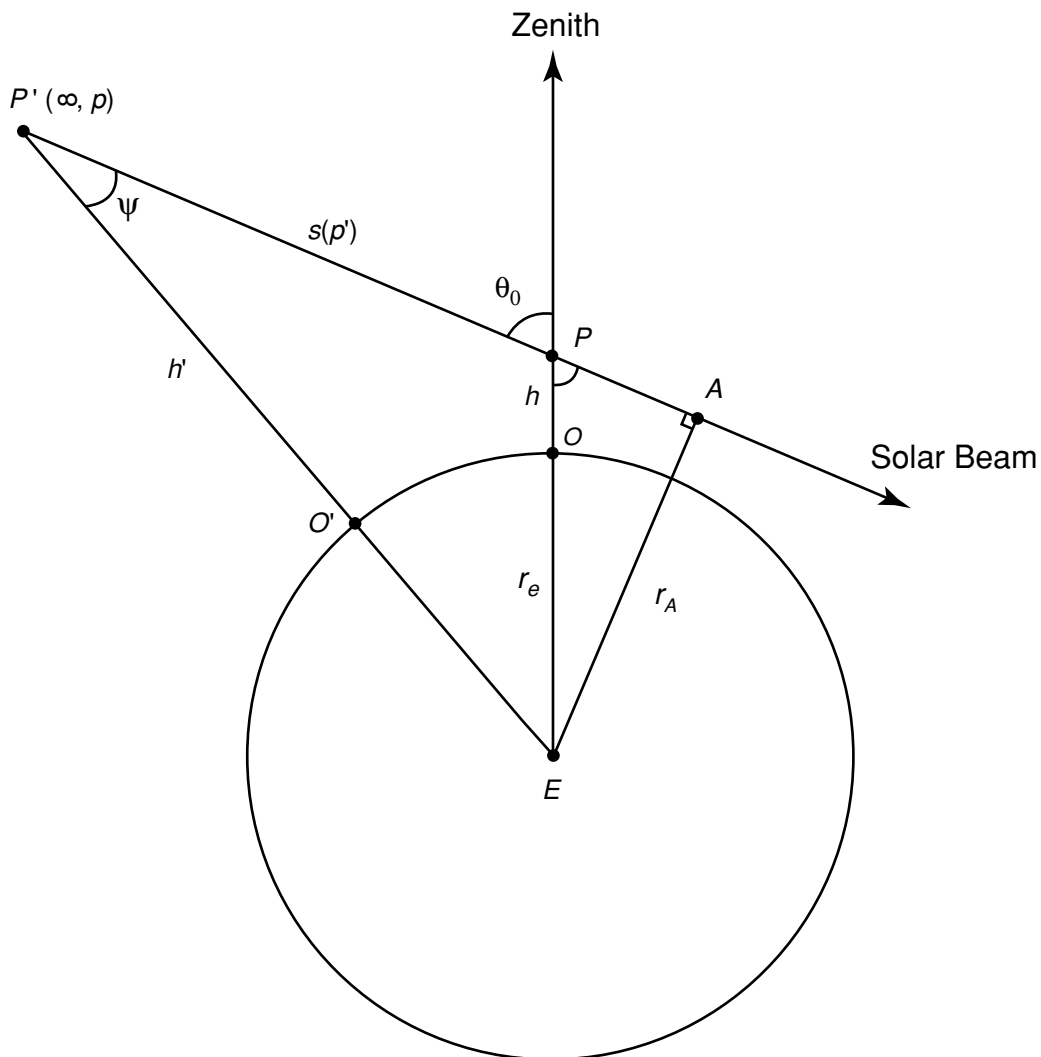


**Figure 3.20**  Spherical geometry for the evaluation of the Chapman function: $\theta_0 =$ solar zenith angle, $r_e =$ earth's radius, $r_A = AE$, $h = PO$, $h' = P'O'$, $s(p') =$ the path length from point $p'$ to $A$. The objective is to compute the absorption at point $P$, which is at a height $h$ above the earth's surface, based on the actual path length $s(p')$.

the limit of the solar zenith angle under which $1/\mu_0$ is a good approximation of the exponential attenuation calculation.

3.4  Given the values of $K_{12} = 5.6 \times 10^{-46}(300/T)^{2.36}\mathrm{m}^6\,\mathrm{sec}^{-1}$ and $K_{13} = 2.0 \times 10^{-17}\exp(-2280/T)\,\mathrm{m}^3\,\mathrm{sec}^{-1}$, and the $J_2$ and $J_3$ values in the following table, compute the equilibrium ozone concentration as a function of height and compare your results with those presented in Fig. 3.8. Use the standard atmospheric temperature and molecular number density profiles (Appendix G) in your calculations.

| Height (km) | 30 | 35 | 40 | 45 | 50 |
|---|---|---|---|---|---|
| $J_2(\mathrm{sec}^{-1}) \times 10^{-10}$ | 0.61 | 2.13 | 4.56 | 7.93 | 11.30 |
| $J_3(\mathrm{sec}^{-1}) \times 10^{-3}$ | 0.62 | 1.09 | 2.03 | 4.31 | 6.29 |

3.5  The principal photochemical reactions involving oxygen in the thermosphere are found to be

$$O_2 + h\tilde{v}(\lambda < 1751 \text{ Å}) \xrightarrow{J_2} O + O,$$

$$O + O + M \xrightarrow{K_{11}} O_2 + M,$$

$$O + O \xrightarrow{K'_{11}} O_2 + h\tilde{v}.$$
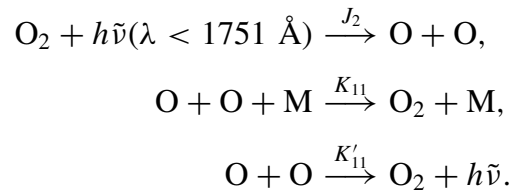
Express these photochemical processes in terms of the rate of change of the number density of O and $O_2$. Derive the number density of O under the photochemical equilibrium condition.

3.6  For very strong Lorentz lines (see Section 1.3.2), the half-width is much smaller than the spread of the line such that $\alpha \ll (\nu - \nu_0)$. Under this condition and using a single line, show that the spectral absorptivity is proportional to the square root of the path length. In your analysis, define the relevant parameters in the wavenumber domain and use the following integration:

$$\int_0^\infty \left(e^{-a^2/x^2} - e^{-b^2/x^2}\right) dx = \sqrt{\pi}(b - a).$$

3.7  The number of molecules per cubic centimeter of air at sea level in standard atmospheric conditions is about $2.55 \times 10^{19}\,\mathrm{cm}^{-3}$. Calculate the scattering cross section of molecules at the 0.3, 0.5, and 0.7 $\mu$m wavelengths.

3.8  The number density profile as a function of height is given by the following table:

| Height (km) | 0 | 2 | 4 | 6 | 8 | 10 | 12 | 14 | 16 |
|---|---|---|---|---|---|---|---|---|---|
| $N(\times 10^{18}\,\mathrm{cm}^{-3})$ | 25.5 | 20.9 | 17.0 | 13.7 | 10.9 | 8.60 | 6.49 | 4.74 | 3.46 |

Calculate the optical depth of a clear atmosphere at the wavelengths shown in Exercise 3.7.

3.9 For all practical purposes, we find that the refractive index $m_r$ and the molecular density $\rho$ are related by

$$(m_r - 1)_{\text{gas}} = \text{const} \times \rho.$$

At sea level, the refractive index of air is about 1.000292 for a wavelength of 0.3 $\mu$m. Find the refractive indices at the heights given in Exercise 3.8. Note that the density (g cm$^{-3}$) is related to the number density $N$(cm$^{-3}$) by $\rho = (M/N_0)N$, where $M$ is the molecular weight of air (28.97 g mol$^{-1}$), and $N_0$ is Avogadro's number (6.02295 $\times 10^{23}$ mol$^{-1}$). Because the refractive index varies with the density of the atmosphere, light rays bend according to the atmospheric density profile and produce a number of atmospheric optical phenomena known as looming, sinking, and superior and inferior mirages.

3.10 An unpolarized ruby laser operated at 0.7 $\mu$m is projected vertically into a clear sky to investigate the density of the atmosphere. A detector located 10 km from the base of the laser is used to receive the flux density scattered from the laser beam by air molecules. Assuming that the laser output has a uniform distribution of flux density $F_0$ across the beam (i.e., $I_0 = F_0/\pi$ sr), and neglecting the effects of multiple scattering, find the scattered flux density at 6 and 10 km received by a detector whose field of view in a plane is 0.05 rad. Use the scattering cross section and molecular density profile obtained from Exercises 3.7 and 3.8.

3.11 (a) The radar backscattering coefficient (in units of per length) for a volume of identical cloud droplets is defined as

$$\beta_\pi = N_c \sigma_\pi = N_c \sigma_s P(\pi),$$

where $N_c$ is the droplet number density, $\sigma_\pi$ the backscattering cross section, and $P(\pi)$ the phase function at backscatter. Employing the Rayleigh scattering cross section and phase function, and noting that $N_c = 1/V$, where the volume of a spherical drop with a radius $a$ is $V = 4\pi a^3/3$, show that

$$\beta_\pi = \frac{64\pi^5}{\lambda^4} N_c a^6 \left| \frac{m^2 - 1}{m^2 + 2} \right|^2.$$

(b) Assuming that the number density and the radius of cloud droplets are 100 cm$^{-3}$ and 20 $\mu$m, respectively, calculate $\beta_\pi$ for the following two radar wavelengths with the corresponding refractive indices for water:

| $\lambda$(cm) | 10 | 3.21 |
|---|---|---|
| $m$ | 3.99–1.47$i$ | 7.14–2.89$i$ |

where $i = \sqrt{-1}$. Compute $\beta_\pi$ again using only the real part of the refractive indices, and show the differences between the two computations.

3.12 From the geometry of a sphere with respect to the incident ray, show that the incident angle $\theta_i$ at which the minimum deviation occurs is given by

$$\cos^2 \theta_i = (m^2 - 1)/(p^2 - 1), \quad p \geq 2,$$

where $(p-1)$ denotes the number of reflection. The refractive index $m$ for water is 1.33 in the visible. Compute the positions defined as the scattering angles for the first and second rainbows.

3.13 From the geometry of a hexagonal plate with respect to the incident ray, show that the angle of refraction at minimum deviation can be determined from

$$\sin\left[\frac{1}{2}(\theta' + A)\right] = m \sin\frac{A}{2},$$

where $A$ denotes the prism angle and the refractive index of ice in the visible is 1.31. For $A = 60°$, $90°$, and $120°$, compute the positions of halos.

3.14 From Eq. (3.3.26), compute and plot the diffraction pattern as a function of $y = x \sin\theta$. What would be the position of the strongest corona produced by uniform-sized aerosols with a radius of 1 $\mu$m? Use a wavelength of 0.5 $\mu$m in your calculation.

3.15 (a) Compute the extinction coefficient as a function of the phase shift parameter, defined in Eqs. (3.3.31) and (3.3.28). (b) Estimate the aerosol particle size under which more blue light is available to an observer than red light based on the first maximum and minimum in the extinction curve assuming a refractive index of 1.5 for aerosols. This is related to an optical phenomenon referred to as *once in a blue moon*. Why is it so rare? Interested readers may also wish to refer to Figs. 5.1 and 5.7 for additional information on aerosol size distribution and extinction.

3.16 Show that for isotropic and Rayleigh scattering cases, the asymmetry factor is zero.

3.17 Consider the cases of pure scattering, referred to as *conservative scattering,* such that $\tilde{\omega} = 1$. Define the net flux associated with the diffuse beam as follows:

$$F(\tau) = \int_0^{2\pi} \int_{-1}^{1} I(\tau, \mu, \phi)\mu \, d\mu \, d\phi.$$

Show from Eq. (3.4.13) that

$$\frac{dF(\tau)}{d\tau} = F_\odot e^{-\tau/\mu_0},$$

and that

$$F(\tau) + \mu_0 F_\odot e^{-\tau/\mu_0} = \text{constant}.$$

This is the so-called *flux integral.* In a pure scattering atmosphere, the total flux (direct plus diffuse solar beam) is conserved.

3.18 From the flux equations given in Eqs. (3.4.13a) and (3.4.13b), derive Eq. (3.4.14).

## Suggested Reading

Brasseur, G., and Solomon, S. (1986). *Aeronomy of the Middle Atmosphere,* 2nd ed. D. Reidel, Dordrecht. Chapter 4 presents a comprehensive discussion of the